ACS APPLIED MATERIALS & INTERFACES

Research Article

www.acsami.org

Strain and Interface Effects in a Novel Bismuth-Based Self-Assembled Supercell Structure

Leigang Li,[†] Wenrui Zhang,[†] Fauzia Khatkhatay,[‡] Jie Jian,[‡] Meng Fan,[‡] Qing Su,[†] Yuanyuan Zhu,[†] Aiping Chen,[‡] Ping Lu,[§] Xinghang Zhang,[∥] and Haiyan Wang*[,†,‡]

[†]Department of Materials Science and Engineering, [‡]Department of Electrical and Computer Engineering, and [∥]Department of Mechanical Engineering, Texas A&M University, College Station, Texas 77843, United States

[§]Sandia National Laboratory, Albuquerque, New Mexico 87185, United States

Supporting Information

ABSTRACT: Bi_2FeMnO_6 (BFMO) thin films with both conventional pseudocubic structure and novel supercell structure have been grown on $SrTiO_3$ (001) substrates with different thicknesses of CeO_2 buffer layers (ranging from 6.7 to 50.0 nm) using pulsed laser deposition. The correlation between the thickness of the CeO_2 buffer layer and the structure of the BFMO films shows that the CeO_2 buffer layer, as thin as 6.7 nm, is sufficient in triggering the novel BFMO supercell structure. This may be ascribed to the interfacial strain between the BFMO supercell structure and the CeO_2 buffer layer which also serves as a seed layer. The buffer layer thickness is found to be critical to control the microstructure and magnetism of the formed BFMO supercell structures. Thin seed layers can produce a smoother interface between the BFMO film and the CeO_2 buffer layer, and therefore better ferrimagnetic properties. Our results have demonstrated that strain and interface could be utilized to generate novel thin film structures and to tune the functionalities of thin films.

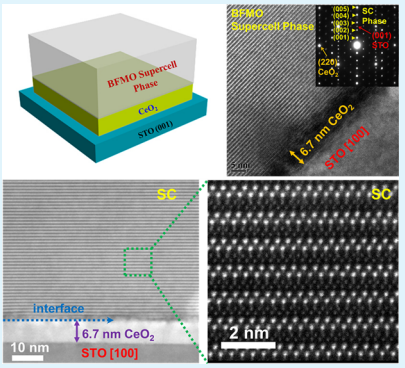

KEYWORDS: *layered oxides, supercell, thin film, strain, interface, ferrimagnetic*

INTRODUCTION

Complex transition metal oxides, including perovskite, double-perovskite, spinel, rocksalt, rutile, etc., have been extensively studied in the past decades.[1−8] The development of state-of-the-art thin film growth techniques and the growing needs for oxide-based functional devices have further stimulated the progress in this field.[9−11] Diversified unique physical properties have been reported, such as magnetoresistance,[12−14] multiferroism,[1,6,15−18] magnetoelectricity,[19,20] and high-temperature superconductivity.[21] These physical properties are strongly correlated to the lattice structures of complex oxides.[12] Among all the factors controlling complex oxide lattice structures, strain has been reported to play a critical role in tailoring the lattice structures and therefore the functionalities of transition metal oxide thin films.[2,22] For example, strain engineering provides an easy and effective way to control the overall film structure and thus tune the physical properties, such as the giant magnetocaloric effect in $La_{0.7}Ca_{0.3}MnO_3$,[23] the enhanced perpendicular magnetic anisotropy in $BiFeO_3$:$CoFe_2O_4$,[24] and the tunable low-field magnetoresistance in $(La_{0.7}Sr_{0.3}MnO_3)_{0.5}$:$(ZnO)_{0.5}$.[12,25]

More attractively, strain engineering could trigger new structures, for example, the intermediate pseudomorphic structures Ti_2O_3 and V_2O_3 have been previously reported in $TiO_2/Ti_2O_3/Al_2O_3$ and $VO_2/V_2O_3/Al_2O_3$ heterostructures,[22,26,27] respectively. Another exciting example is the formation of the novel self-assembled $Bi_3Fe_2Mn_2O_x$ supercell (BFMO322 SC), which was enabled by the careful selection of substrates and deposition parameters.[22,28] It is a novel layered oxide structure that is formed on $LaAlO_3$ (LAO) substrates, and exhibits superior multiferroic properties at room temperature with the saturation magnetization value of 110 emu/cc. Strain was found to play a critical role in the formation of the new BFMO322 SC structure.[22,28] Comparing the lattice mismatch between the $SrTiO_3$ (STO) substrate and the BFMO pseudocubic structure (−0.6%) with that between LAO and BFMO322 SC (−2.0%), the later exhibits a much larger lattice mismatch which could be the primary reason triggering the formation of a thin strained transition layer (∼5 nm) before the formation of the supercell phase. This reassembles the characteristics of a typical pseudomorphic growth in thin film epitaxy, i.e., a thin layer of highly strained layer was formed within a critical thickness and beyond that, the film is relaxed with misfit dislocations nucleated at the transition interface.[26,27] However, the BFMO322 SC case is much more complicated with a new phase formation and the strain relaxation mechanism is thus quite different from the simple nucleation of misfit dislocations.

To explore the formation mechanism of the BFMO322 SC structure, a unique approach could be used to grow the critical

Received: March 29, 2015
Accepted: May 8, 2015
Published: May 8, 2015

DOI: 10.1021/acsami.5b02699
ACS Appl. Mater. Interfaces 2015, 7, 11631−11636

transition layer with various film thicknesses, and explore the corresponding phase transformation. Here we select a CeO_2 buffer layer as the critical transition layer. We have demonstrated that a thin layer of CeO_2 could also serve as an excellent buffer layer enabling the growth of BFMO322 SC. This is because a 45° in-plane rotated CeO_2 (a = 5.411 Å, $a/\sqrt{2}$ = 3.826 Å) provides a perfect lattice match for the growth of the BFMO322 SC phase on $SrTiO_3$ substrates (a = 3.905 Å). In this study, the effects of the strain and the interface structure of the CeO_2 buffer layer on the microstructure and ferrimagnetic property of BFMO films were investigated by systematically controlling the CeO_2 buffer layer thickness. The results could shed light on the supercell growth mechanisms that can be generalized to other supercell systems for new functionalities.

EXPERIMENTAL SECTION

The composite BFMO and the CeO_2 targets were prepared by a conventional solid state sintering method. For the BFMO target, the powders of Bi_2O_3, Fe_2O_3 and MnO_2 were mixed in stoichiometric ratio, pressed into a pellet, and then sintered at 800 °C for 3 h. For CeO_2 target, the powder of CeO_2 was pressed into a pellet and annealed at 1200 °C for 6 h. The growth of BFMO films and CeO_2 buffer layers was conducted using pulsed laser deposition (PLD) under an optimized substrate temperature of 700 °C and an oxygen pressure of 200 mTorr. After deposition, the films were in situ annealed at 400 °C for 1 h with an oxygen pressure of 500 Torr and then cooled down to room temperature with a cooling rate of 5 °C/min.

The microstructures of the films were investigated by high resolution X-ray diffraction (HRXRD, PANalytical Empyrean) and transmission electron microscopy (TEM, FEI Tecnai G2 F20). The high resolution scanning transmission electron microscopy (HRSTEM) images in high angle annular dark-field (HAADF) mode (also called Z-contrast imaging) were obtained using a FEI Titan G2 80–200 STEM with a Cs probe corrector operated at 200 kV and a modified FEI Titan STEM TEAM 0.5 with a convergence semiangle of 17 mrad operating at 300 kV. The magnetic properties of the films were investigated using the vibrating sample magnetometer (VSM) option in a commercial physical properties measurement system (PPMS 6000, Quantum Design). During measurements, the out-of-plane and in-plane magnetization were recorded by applying a magnetic field of 1 T perpendicular and parallel to the film plane, respectively.

RESULTS AND DISCUSSION

Figure 1 shows the θ–2θ XRD patterns of the BFMO films directly on STO and on CeO_2 buffered STO substrates. Figure 1a indicates the high quality textured growth of BFMO pseudocubic structure along the (00l) direction of STO as evidenced by the dominant BFMO (00l) diffractions. Significantly different from the pseudocubic structure directly grown on STO, however, a new set of (00l) peaks along with CeO_2 (002) and (004) peaks appear when the film was deposited on STO substrate buffered by 6.7 nm CeO_2 as shown in Figure 1b. This new set of diffractions belongs to the layered BFMO322 SC structure which is composed of Bi_2O_2 sheets and distorted FeO_6/MnO_6 octahedra[22] as shown by the high resolution STEM image of the supercell structure in Figure 2a, b. The bright sheets in Figure 2a are attributed to the Bi_2O_2 because of the heavier element of Bi (Z_{Bi} = 83) than that of Fe (Z_{Fe} = 26) and Mn (Z_{Mn} = 25).[24] Figure 2b clearly shows the bright zigzag Bi_2O_2 sheets as well as the less bright distorted FeO_6/MnO_6 octahedra. For the composition of the BFMO thin films, dispersive X-ray spectroscopy (EDS) analysis was conducted and showed that there is about 9% bismuth loss

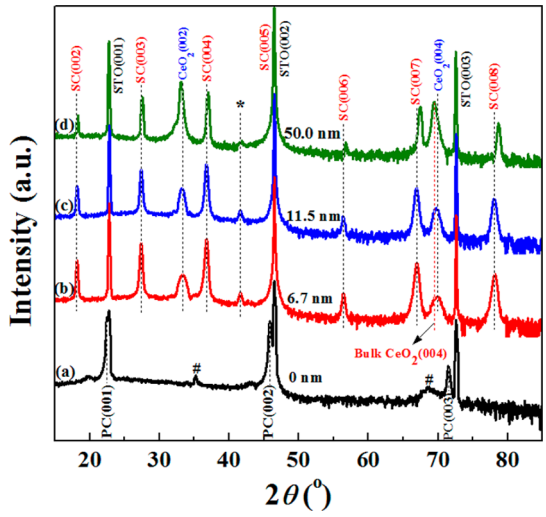

Figure 1. (a) XRD θ–2θ scans of BFMO film directly grown on STO substrate with a pseudo-cubic structure. The "#" indicates impurity phase and PC means pseudo-cubic phase. (b–d) XRD scans of the BFMO322 SC structure grown on STO substrates buffered by different thicknesses of CeO_2 ranging from 6.7, 11.5, to 50.0 nm, respectively. The "*" indicates a minor unidentified phase.

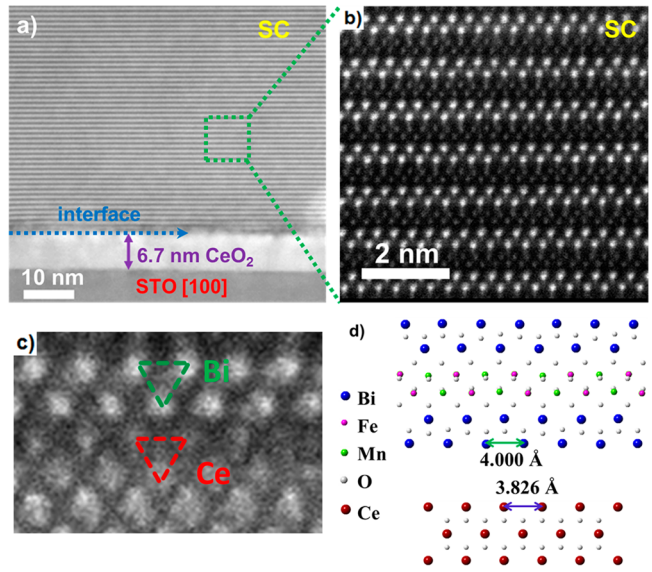

Figure 2. Cross-sectional STEM image of the 6.7 nm CeO_2 buffered BFMO322 SC with (a) low-magnification and (b) high-magnification, (c) STEM image of the interface between BFMO322 SC and CeO_2, (d) schematic modeling showing the interface lattice matching between BFMO322 SC and CeO_2.

for the conventional pseudocubic phase, whereas the cation ratio of the novel supercell phase is Bi:Fe:Mn = 3:2:2, with higher bismuth loss. This is also confirmed by the atomic model built for the supercell structure based on the previous report.[22] As the CeO_2 thickness increases to 11.5 and 50.0 nm, similar XRD results to that of Figure 1b have been obtained as shown in Figure 1c, d, respectively. It is interesting to note that the peaks of the CeO_2 buffer layer shift to the left while the new supercell structure shifts to the right with increasing the CeO_2 thickness. For example, the CeO_2 (004) peak shifts from 69.80 to 69.40° and SC (008) peak shifts from 78.10 to 78.65° when the CeO_2 thickness increases from 6.7 to 50.0 nm. For the left shift of the CeO_2 peaks, it could be attributed to that, with the

DOI: 10.1021/acsami.5b02699
ACS Appl. Mater. Interfaces 2015, 7, 11631–11636

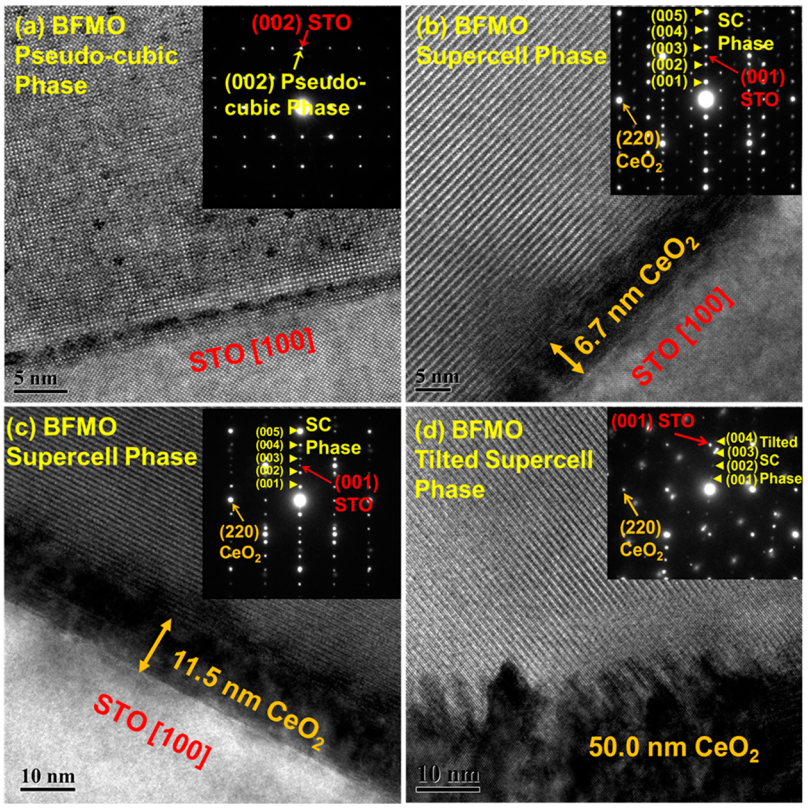

Figure 3. Cross-sectional TEM images and diffraction patterns of the BFMO samples (along (100) zone axis). (a) BFMO with pseudo-cubic structure. (b–d) BFMO322 SC structure with the CeO_2 thickness of 6.7, 11.5, and 50.0 nm, respectively.

increase of the CeO_2 thickness from 6.7 to 50.0 nm, the strain generated from the substrate is relaxed as shown by the red dashed line for bulk CeO_2 (004) peak in Figure 1. For the right shift of the supercell peaks buffered by 50.0 nm CeO_2, it is to be discussed in the later part.

To better understand the microstructure evolution as a function of the CeO_2 buffer layer thickness, cross-sectional TEM was conducted for both the BFMO films grown on STO only and CeO_2-buffered STO substrates, as shown in Figure 3. Figure 3a shows the cross-sectional TEM image of the BFMO film directly grown STO substrate with the pseudocubic structure. The corresponding selected area diffraction (SAED) pattern shown as the inset in Figure 3a clearly illustrates the pseudocubic structure and high-quality epitaxy of the film with clear cubic lattice fringes. Completely different from the pseudocubic BFMO structure directly grown on STO substrate; however, a distinctively new layered structure (BFMO322 SC) is formed on the 6.7 nm CeO_2 buffered STO substrates, as shown in Figures 2b and 3b. The distinguished diffraction dots in the inset of Figure 3b indicate the highly epitaxial growth of the BFMO322 SC structure. For the two distinctively different BFMO structures, the strain mapping analysis of these two structures has shown that strain may play an indispensable role in triggering the formation of the supercell structure.[28] As discussed above, the strain between the BFMO film and the STO substrate is only −0.6%, whereas it is −2.0% for the BFMO film and the LAO substrate. The relatively small lattice mismatch between the BFMO film and the STO substrate has enabled the cube-on-cube growth. The much larger lattice mismatch between BFMO film and LAO substrate, however, leads to the growth of highly distorted pseudocubic structure, forming a thin transition layer. With the increase of film thickness, the large strain in the transition layers gets relaxed followed by the formation of the novel layered structure. For the CeO_2 buffered BFMO samples in this work, the 45°-rotated CeO_2 provides an optimal lattice match between CeO_2 and BFMO322 SC and the strain is calculated to be about −4.4% between CeO_2 and BFMO322 SC (Figure 2c, d). Furthermore, the zigzagged Ce–Ce layer has served as an ideal template for the following Bi–Bi layer. Overall, both the large strain between CeO_2 and BFMO322 SC and the zigzagged Ce–Ce bonding structure have triggered the formation of the BFMO322 SC.

For the 11.5 nm CeO_2 buffered case, a similar quality of BFMO film with distinctive diffraction patterns was obtained (Figure 3c), except a small amount of tilted supercell growth observed in few areas (Figure S1 in the Supporting Information). When the thickness of the CeO_2 buffer layer was increased to 50.0 nm, the film quality of both the CeO_2 buffer layer and the BFMO film is distinctively lower than those of the thinner buffer layer cases, as shown by Figure 3d. The interface between the BFMO film and the CeO_2 buffer layer is no longer smooth as that in Figure 3b, c and the Bi_2O_2 lattices of the supercell are not parallel to the surface of the STO substrate. Instead, the Bi_2O_2 lattices form a certain angle with the lattice of the STO substrate. This tilted supercell structure is quite different from the 6.7 and 11.5 nm CeO_2 buffered samples and thus results in different peak positions in XRD results (Figure 1). The microstructure evolution of BFMO films with the increase of the CeO_2 buffer layer thickness could be correlated to the strain state of the CeO_2 buffer layer and the interface morphology between the BFMO film and the CeO_2 buffer layer. The interface between the BFMO film and the CeO_2 buffer layer of the 6.7 nm CeO_2 buffered sample is sharp

DOI: 10.1021/acsami.5b02699
ACS Appl. Mater. Interfaces 2015, 7, 11631–11636

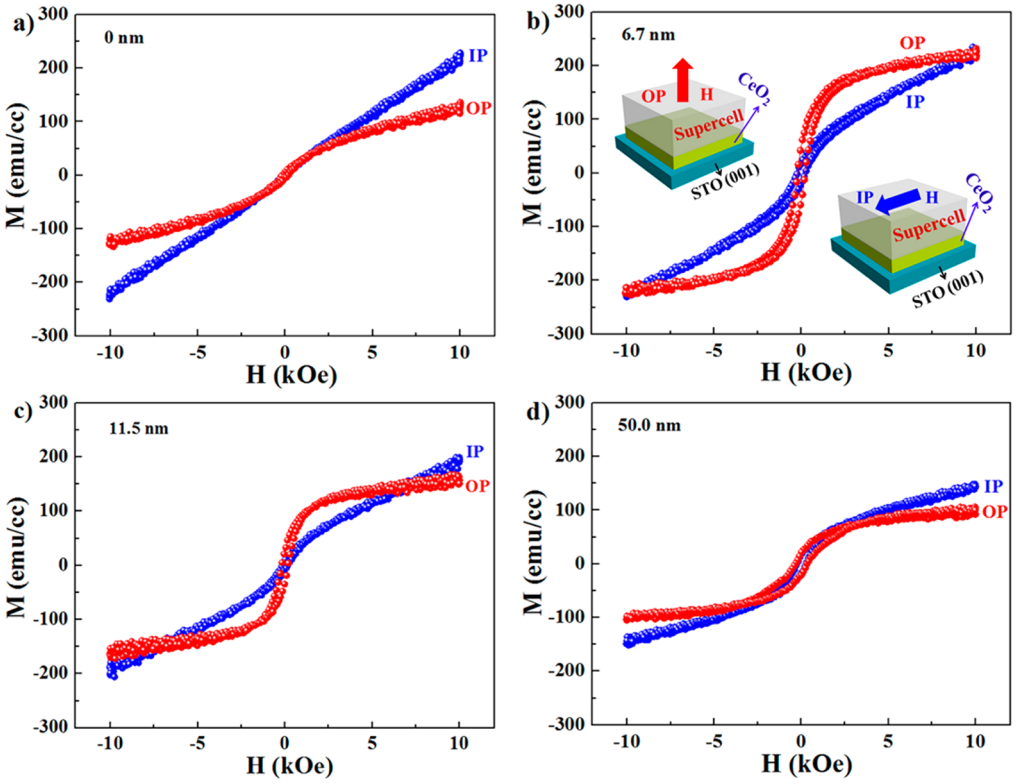

Figure 4. Room-temperature magnetic properties of the BFMO films. (a) Out-of-plane (OP) and in-plane (IP) magnetic hysteresis loops of the BFMO film with pseudo-cubic structure. (b–d) OP and IP magnetic hysteresis loops of the BFMO322 SC structure grown on STO substrates buffered by different thicknesses of CeO_2 ranging from 6.7, 11.5, to 50.0 nm, respectively.

and smooth (Figures 2a and 3b) because of the layer-by-layer growth of the strained CeO_2 buffer layer with the in-plane 45° rotation on STO. This smooth interface has served as an optimal surface seed layer to trigger the growth of the highly epitaxial supercell structure with the Bi_2O_2 sheets parallel to the surface of the STO substrate. The film structure and the interface of the 11.5 nm CeO_2 buffered sample resembles that of the 6.7 nm CeO_2 buffered sample except that tilted supercell phase has been observed in some areas (Figure S1 in the Supporting Information) due to the island growth of the CeO_2 buffer layer initiated around this CeO_2 thickness. The growth of the tilted supercell become dominant for the 50.0 nm CeO_2 buffered sample (Figure 3d and Figure S2 in the Supporting Information). This could be ascribed to the rough interface due to the dominant island growth of the CeO_2 buffer layer. Owing to the island morphology of the CeO_2 buffer layer, the BFMO322 SC lattice has coupled to island lattice facets which could trigger the tilted growth of the supercell. Overall the above findings suggest the CeO_2 buffer layer thickness plays a critical role in the film strain, surface morphology, and the resulting film structures.

To reveal the structure–property correlation of the BFMO films, we obtained room-temperature (300 K) magnetic hysteresis loops by applying magnetic field perpendicular (out-of-plane, OP) and parallel (in-plane, IP) to the film surface as shown in Figure 4. By comparing the out-of-plane magnetic hysteresis of the BFMO films directly deposited on STO with that on CeO_2 buffered STO, it is obvious that the supercell structure grown on the CeO_2 buffer layer is superior to the conventional pseudocubic structure. From Figure 4b, it is clearly shown that the BFMO film with a 6.7 nm CeO_2 buffer layer has a higher out-of-plane saturation magnetization value of about 226 emu/cc than that of the BFMO sample with the pseudocubic structure (126 emu/cc in Figure 4a) in this work. This result clearly suggests the superior magnetic properties of the novel self-assembled supercell structure. Furthermore, the 6.7 nm CeO_2 buffered sample shows a strong magnetic anisotropy, which benefits the high-density magnetic memory device applications. The much stronger magnetization and distinguished magnetic anisotropy of the supercell structure could be attributed to the strong anisotropic layered structure and the resulted highly anisotropic properties. Coupled with the ferroelectric properties from the previous report,[22] the remnant polarization value P_r is 6.0 $\mu C/cm^2$ for the novel BFMO supercell phase while the conventional BFMO phase showed a P_r of 2.7 $\mu C/cm^2$. Although its P_r value is lower than that of other ferroelectric materials, such as $BiFeO_3$ with P_r of 60–80 $\mu C/cm^2$, the supercell structure with CeO_2 buffer showed a much stronger room temperature magnetization of 226 emu/cc compared to $BiFeO_3$ (<40 emu/cc).

It is noted that with the increase in CeO_2 buffer layer thickness, the saturation magnetization values decrease. For example, when the CeO_2 thickness increases to 11.5 nm, the supercell structure exhibits a relatively lower out-of-plane saturation magnetization value of 161.9 emu/cc. This lowered saturation magnetization value could be related to the tilted supercell structure in certain areas of the film (Figure S1 in the Supporting Information). For the sample with 50.0 nm CeO_2 buffer layer, it shows the lowest saturation magnetization value and magnetic hysteresis anisotropy among all the supercell structures. In this case, the interface between the film and the CeO_2 buffer layer is no longer as smooth as that in the other samples and a large amount of tilted supercell phase exists (Figure 3d and Figure S2 in the Supporting Information). This

DOI: 10.1021/acsami.5b02699
ACS Appl. Mater. Interfaces 2015, 7, 11631–11636

results in a much lower saturation value and magnetic anisotropy. There is a concern on the possible magnetic properties introduced by the CeO_2 layer, since CeO_2 with high density Ce and/or oxygen vacancies has been reported to be ferromagnetic by previous reports.[29,30] However, in this case, the magnetism contribution from CeO_2 is minimal as the CeO_2 layer is thin and the films have minimum amount of oxygen vacancies due to the postdeposition annealing procedure.

The variation of the magnetic property as a function of the CeO_2 buffer thickness is also consistent with the above TEM, STEM, and XRD results. These results indicate that a critical thickness range for the CeO_2 buffer layer is required for the formation of the smooth interface and thus the high phase purity and high epitaxial quality of the BFMO322 SC structure. The 6.7 nm CeO_2 buffer layer is the optimal condition with a smooth interface between the supercell structure and the CeO_2 buffer layer and the optimal seed layer pattern for the formation of highly epitaxial BFMO322 SC structure with the highest saturation magnetization value and magnetic anisotropy. This clearly suggests the advantage of the CeO_2 buffer layer in enabling the formation of novel supercell structure with enhanced magnetic properties. The correlation between the magnetic properties and the structures of the BFMO films has demonstrated the important role of the interface and strain in tailoring the microstructure of the film as well as tuning the physical properties.

CONCLUSIONS

In summary, the thickness dependence effects of the CeO_2 buffer layer on the microstructure and magnetic properties of the BFMO films have been studied. Without the CeO_2 buffer layer, a conventional pseudocubic structure has been obtained on STO substrate with a minimum saturation magnetization value. When buffered by CeO_2, a novel layered supercell structure forms because of the strain and surface structure induced by the CeO_2 buffer layer. The magnetic property measurement shows that the novel supercell structure with the optimal CeO_2 buffer layer thickness of 6.7 nm exhibits significantly enhanced magnetic properties compared to the conventional pseudocubic structure without the CeO_2 buffer. Moreover, it has been demonstrated that the interface morphology between the BFMO and CeO_2 layers plays a crucial role in the formation of the supercell structure with superior magnetic property. This study demonstrates that both strain and interface can be used to tune the structural and physical properties of the transition metal oxide thin films for novel structures and new functionalities.

ASSOCIATED CONTENT

Supporting Information

Cross-sectional TEM images of 11.5 and 50.0 nm CeO_2 buffered samples showing the tilted supercell phase and island morphology of CeO_2. The Supporting Information is available free of charge on the ACS Publications website at DOI: 10.1021/acsami.5b02699.

AUTHOR INFORMATION

Corresponding Author

*E-mail: wangh@ece.tamu.edu.

Notes

The authors declare no competing financial interest.

ACKNOWLEDGMENTS

This work was supported by the U.S. Office of Naval Research (under the supervision of Dr. Brian R. Bennett). H.W., W.Z., and J.J. acknowledge the support from the U.S. National Science Foundation (Grant DMR-0846504 and DMR-1401266) for high-resolution TEM/STEM analysis. Sandia National Laboratories is a multiprogram laboratory managed and operated by Sandia Corporation, a wholly owned subsidiary of Lockheed Martin Corporation, for the U.S. Department of Energy's National Nuclear Security Administration under contract DE-AC04-94AL85000. A portion of the electron microscopy experiments were performed at the National Center for Electron Microscopy, Molecular Foundry, which is supported by the Office of Science, Office of Basic Energy Sciences of the U.S. Department of Energy under Contract No. DE-AC02-5CH11231. L.L. gratefully acknowledges the financial support from the China Scholarship Council (CSC).

REFERENCES

(1) Wang, J.; Neaton, J. B.; Zheng, H.; Nagarajan, V.; Ogale, S. B.; Liu, B.; Viehland, D.; Vaithyanathan, V.; Schlom, D. G.; Waghmare, U. V.; Spaldin, N. A.; Rabe, K. M.; Wuttig, M.; Ramesh, R. Epitaxial $BiFeO_3$ Multiferroic Thin Film Heterostructures. *Science* **2003**, *299*, 1719−1722.

(2) MacManus-Driscoll, J. L.; Zerrer, P.; Wang, H.; Yang, H.; Yoon, J.; Fouchet, A.; Yu, R.; Blamire, M. G.; Jia, Q. Strain Control and Spontaneous Phase Ordering in Vertical Nanocomposite Heteroepitaxial Thin Films. *Nat. Mater.* **2008**, *7*, 314−320.

(3) Khatkhatay, F.; Chen, A.; Lee, J. H.; Zhang, W.; Abdel-Raziq, H.; Wang, H. Ferroelectric Properties of Vertically Aligned Nanostructured $BaTiO_3$-CeO_2 Thin Films and Their Integration on Silicon. *ACS Appl. Mater. Interfaces* **2013**, *5*, 12541−12547.

(4) Du, Y.; Cheng, Z. X.; Dou, S. X.; Wang, X. L.; Zhao, H. Y.; Kimura, H. Magnetic Properties of Bi_2FeMnO_6: A Multiferroic Material with Double-Perovskite Structure. *Appl. Phys. Lett.* **2010**, *97*, 122502.

(5) Bi, Z.; Lee, J. H.; Yang, H.; Jia, Q.; MacManus-Driscoll, J. L.; Wang, H. Tunable Lattice Strain in Vertically Aligned Nanocomposite $(BiFeO_3)_x$:$(Sm_2O_3)_{1-x}$ Thin Films. *J. Appl. Phys.* **2009**, *106*, 094309.

(6) Zheng, H.; Wang, J.; Lofland, S. E.; Ma, Z.; Mohaddes-Ardabili, L.; Zhao, T.; Salamanca-Riba, L.; Shinde, S. R.; Ogale, S. B.; Bai, F.; Viehland, D.; Jia, Y.; Schlom, D. G.; Wuttig, M.; Roytburd, A.; Ramesh, R. Multiferroic $BaTiO_3$-$CoFe_2O_4$ Nanostructures. *Science* **2004**, *303*, 661−663.

(7) Luo, H.; Yang, H.; Baily, S. A.; Ugurlu, O.; Jain, M.; Hawley, M. E.; McCleskey, T. M.; Burrell, A. K.; Bauer, E.; Civale, L.; Holesinger, T. G.; Jia, Q. Self-Assembled Epitaxial Nanocomposite $BaTiO_3$-$NiFe_2O_4$ Films Prepared by Polymer-Assisted Deposition. *J. Am. Chem. Soc.* **2007**, *129*, 14132−14133.

(8) Jian, J.; Chen, A.; Zhang, W.; Wang, H. Sharp Semiconductor-to-Metal Transition of VO_2 Thin Films on Glass Substrates. *J. Appl. Phys.* **2013**, *114*, 244301.

(9) Chen, A.; Bi, Z.; Jia, Q.; MacManus-Driscoll, J. L.; Wang, H. Microstructure, Vertical Strain Control and Tunable Functionalities in Self-Assembled, Vertically Aligned Nanocomposite Thin Films. *Acta. Mater.* **2013**, *61*, 2783−2792.

(10) Zhang, W.; Chen, A.; Bi, Z.; Jia, Q.; MacManus-Driscoll, J. L.; Wang, H. Interfacial Coupling in Heteroepitaxial Vertically Aligned Nanocomposite Thin Films: From Lateral to Vertical Control. *Curr. Opin. Solid State Mater. Sci.* **2014**, *18*, 6−18.

(11) Ramesh, R.; Spaldin, N. A. Multiferroics: Progress and Prospects in Thin Films. *Nat. Mater.* **2007**, *6*, 21−29.

(12) Chen, A.; Bi, Z.; Tsai, C.-F.; Lee, J.; Su, Q.; Zhang, X.; Jia, Q.; MacManus-Driscoll, J. L.; Wang, H. Tunable Low-Field Magnetoresistance in $(La_{0.7}Sr_{0.3}MnO_3)_{0.5}$:$(ZnO)_{0.5}$ Self-Assembled Vertically

DOI: 10.1021/acsami.5b02699
ACS Appl. Mater. Interfaces 2015, 7, 11631−11636

Aligned Nanocomposite Thin Films. *Adv. Funct. Mater.* **2011**, *21*, 2423−2429.
(13) Chen, A.; Weigand, M.; Bi, Z.; Zhang, W.; Lu, X.; Dowden, P.; MacManus-Driscoll, J. L.; Wang, H.; Jia, Q. Evolution of Microstructure, Strain and Physical Properties in Oxide Nanocomposite Films. *Sci. Rep.* **2014**, *4*, 5426.
(14) Chen, A.; Zhang, W.; Jian, J.; Wang, H.; Tsai, C.-F.; Su, Q.; Jia, Q.; MacManus-Driscoll, J. L. Role of Boundaries on Low-Field Magnetotransport Properties of $La_{0.7}Sr_{0.3}MnO_3$-Based Nanocomposite Thin Films. *J. Mater. Res.* **2013**, *28*, 1707−1714.
(15) Yang, H.; Wang, H.; Yoon, J.; Wang, Y.; Jain, M.; Feldmann, D. M.; Dowden, P. C.; MacManus-Driscoll, J. L.; Jia, Q. Vertical Interface Effect on the Physical Properties of Self-Assembled Nanocomposite Epitaxial Films. *Adv. Mater.* **2009**, *21*, 3794−3798.
(16) Wu, J.; Wang, J.; Xiao, D.; Zhu, J. Migration Kinetics of Oxygen Vacancies in Mn-Modified $BiFeO_3$ Thin Films. *ACS Appl. Mater. Interfaces* **2011**, *3*, 2504−2511.
(17) Wu, J.; Wang, J.; Xiao, D.; Zhu, J. Ferroelectric Behavior in Bismuth Ferrite Thin Films of Different Thickness. *ACS Appl. Mater. Interfaces* **2011**, *3*, 3261−3263.
(18) Wu, J.; Wang, J.; Xiao, D.; Zhu, J. A Method to Improve Electrical Properties of $BiFeO_3$ Thin Films. *ACS Appl. Mater. Interfaces* **2012**, *4*, 1182−1185.
(19) Eerenstein, W.; Mathur, N. D.; Scott, J. F. Multiferroic and Magnetoelectric Materials. *Nature* **2006**, *442*, 759−765.
(20) Spaldin, N. A.; Fiebig, M. The Renaissance of Magnetoelectric Multiferroics. *Science* **2005**, *309*, 391−392.
(21) Logvenov, G.; Gozar, A.; Bozovic, I. High-Temperature Superconductivity in a Single Copper-Oxygen Plane. *Science* **2009**, *326*, 699−702.
(22) Chen, A.; Zhou, H.; Bi, Z.; Zhu, Y.; Luo, Z.; Bayraktaroglu, A.; Phillips, J.; Choi, E.-M.; MacManus-Driscoll, J. L.; Pennycook, S. J.; Narayan, J.; Jia, Q.; Zhang, X.; Wang, H. A New Class of Room-Temperature Multiferroic Thin Films with Bismuth-Based Supercell Structure. *Adv. Mater.* **2013**, *25*, 1028−1032.
(23) Moya, X.; Hueso, L. E.; Maccherozzi, F.; Tovstolytkin, A. I.; Podyalovskii, D. I.; Ducati, C.; Phillips, L. C.; Ghidini, M.; Hovorka, O.; Berger, A.; Vickers, M. E.; Defay, E.; Dhesi, S. S.; Mathur, N. D. Giant and Reversible Extrinsic Magnetocaloric Effects in $La_{0.7}Ca_{0.3}MnO_3$ Films Due to Strain. *Nat. Mater.* **2013**, *12*, 52−58.
(24) Zhang, W.; Jian, J.; Chen, A.; Jiao, L.; Khatkhatay, F.; Li, L.; Chu, F.; Jia, Q.; MacManus-Driscoll, J. L.; Wang, H. Strain Relaxation and Enhanced Perpendicular Magnetic Anisotropy in $BiFeO_3$:$CoFe_2O_4$ Vertically Aligned Nanocomposite Thin Films. *Appl. Phys. Lett.* **2014**, *104*, 062402.
(25) Zhang, W.; Chen, A.; Khatkhatay, F.; Tsai, C.-F.; Su, Q.; Jiao, L.; Zhang, X.; Wang, H. Integration of Self-Assembled Vertically Aligned Nanocomposite $(La_{0.7}Sr_{0.3}MnO_3)_{1-x}$:$(ZnO)_x$ Thin Films on Silicon Substrates. *ACS Appl. Mater. Interfaces* **2013**, *5*, 3995−3999.
(26) Bayati, M. R.; Molaei, R.; Narayan, R. J.; Narayan, J.; Zhou, H.; Pennycook, S. J. Domain Epitaxy in TiO_2/α-Al_2O_3 Thin Film Heterostructures with Ti_2O_3 Transient Layer. *Appl. Phys. Lett.* **2012**, *100*, 251606.
(27) Narayan, J.; Larson, B. C. Domain Epitaxy: A Unified Paradigm for Thin Film Growth. *J. Appl. Phys.* **2003**, *93*, 278−285.
(28) Zhu, Y.; Chen, A.; Zhou, H.; Zhang, W.; Narayan, J.; MacManus-Driscoll, J. L.; Jia, Q.; Wang, H. Research Updates: Epitaxial Strain Relaxation and Associated Interfacial Reconstructions: The Driving Force for Creating New Structures with Integrated Functionality. *APL Mater.* **2013**, *1*, 050702.
(29) Fernandes, V.; Mossanek, R. J. O.; Schio, P.; Klein, J. J.; de Oliveira, A. J. A.; Ortiz, W. A.; Mattoso, N.; Varalda, J.; Schreiner, W. H.; Abbate, M.; Mosca, D. H. Dilute-Defect Magnetism: Origin of Magnetism in Nanocrystalline CeO_2. *Phys. Rev. B* **2009**, *80*, 035202.
(30) Chen, S.-Y.; Tsai, C.-H.; Huang, M.-Z.; Yan, D.-C.; Huang, T.-W.; Gloter, A.; Chen, C.-L.; Lin, H.-J.; Chen, C.-T.; Dong, C.-L. Concentration Dependence of Oxygen Vacancy on the Magnetism of CeO_2 Nanoparticles. *J. Phys. Chem. C* **2012**, *116*, 8707−8713.

DOI: 10.1021/acsami.5b02699
ACS Appl. Mater. Interfaces 2015, 7, 11631−11636